Jiang et al. *Zool. Res.* 2026, 47(1): 128−138
https://doi.org/10.24272/j.issn.2095-8137.2025.282
https://cstr.cn/32248.14.zr.2025.282

ZR | Zoological Research

Article Open Access

Vertebral morphological changes driven by *rflna* lead to body shape differentiation in carp

Zhou Jiang[1,2,#], Bi-Jun Li[1,2,#], Lin Chen[1,2,3,#], Ning Li[1], Shui-Mu Hu[1], Jing-Xin Ma[1], Bin-Ruo Wang[1], Fei Pu[1], Jian Xu[4], Yan-Hui Wang[5], Jian-Xin Feng[5], Xue-Jun Li[6], Tao Zhou[1,2,*], Peng Xu[1,2,*]

[1] *State Key Laboratory of Mariculture Breeding*, *College of Ocean and Earth Sciences*, *Xiamen University*, *Xiamen*, *Fujian* 361102, *China*

[2] *Fujian Key Laboratory of Genetics and Breeding of Marine Organisms*, *College of Ocean and Earth Sciences*, *Xiamen University*, *Xiamen*, *Fujian* 361102, *China*

[3] *State Key Laboratory of Marine Environmental Science*, *College of Ocean and Earth Sciences*, *Xiamen University*, *Xiamen*, *Fujian* 361102, *China*

[4] *Fisheries Engineering Institute*, *Chinese Academy of Fishery Sciences*, *Beijing* 100141, *China*

[5] *Henan Academy of Fishery Sciences*, *Zhengzhou*, *Henan* 450039, *China*

[6] *College of Fisheries*, *Henan Normal University*, *Xinxiang*, *Henan* 453007, *China*

ABSTRACT

Body shape evolution in vertebrates frequently involves modifications in vertebral number or patterns of vertebral fusion, with distinct lineages displaying divergent trajectories. This study investigated the morphological and genetic basis of body shape variation between Hebao red carp (HB, *Cyprinus carpio wuyuanensis*) and Yellow River carp (YR, *Cyprinus carpio haematopterus*). Although both subspecies share an identical vertebral count (35), the compressed morphology of HB was attributable to skeletal anomalies, including vertebral shortening and fusion. Genome-wide association and population genetic analyses were performed on F1 and F2 hybrid cohorts to identify loci associated with this phenotype. A total of 231 selective sweep regions were detected across chromosomes A06, A08, A16, B05, and B06, with a prominent locus on chromosome A08 (15.99–16.39 Mb) strongly correlated with body shape traits. Transcriptomic analysis revealed haplotype-dependent expression of *rflna* within this interval, implicating *rflna* in axial skeletal patterning. Functional validation using CRISPR/Cas9-mediated knockout of *rfln* in zebrafish (*Danio rerio*) induced vertebral malformations, including axial shortening, kyphosis, fusion, and a rounded abdominal profile. These results delineate the morphological and molecular framework governing axial remodeling in HB and highlight a conserved regulatory role for *rflna* in teleost skeletal development.

Keywords: Body shape; Hebao red carp; Yellow River carp; Skeletal development; *rflna*

INTRODUCTION

Domesticated taxa have long provided tractable systems for resolving the genetic basis of phenotypic variation. Over the past two decades, molecular studies have increasingly focused on the inheritance and evolutionary dynamics of traits shaped by artificial selection during domestication (Larson et al., 2014). Body shape serves as a key morphological axis for interpreting developmental constraint and evolutionary plasticity under domestication (Blanckenhorn, 2000; Clauset & Erwin, 2008). In teleosts, canonical body forms include fusiform, laterally compressed, dorsoventrally flattened, cylindrical, spherical, ribbon-like, and asymmetrical morphotypes (Hoare et al., 2000). However, selective pressures imposed by captive environments often drive substantial divergence from wild-type morphology. Even within a single species, domesticated lineages may exhibit pronounced variation in body architecture, with consequences for swimming ability, feeding efficiency, and predator avoidance (Pulcini et al., 2013; Wringe et al., 2016).

Body shape variation is widely recognized as a complex quantitative trait governed by the combined effects of multiple loci distributed across the genome (Pang, 1992). To date, several genes involved in skeletal development pathways, including *bmp7* (Jena et al., 1997), *hox* (Wellik, 2007), *wnt3a*

Received: 06 August 2025; Accepted: 27 August 2025; Online: 28 August 2025

Foundation items: This work was supported by the National Natural Science Foundation of China (National Science Fund for Distinguished Young Scholars, National Science Fund for Excellent Young Scholars) (32225049, 31422057), National Key R&D Program of China (2019YFE0119000), Postdoctoral Fellowship Program of CPSF (GZB20230386), and Outstanding Postdoctoral Scholarship, State Key Laboratory of Marine Environmental Science at Xiamen University

[#]Authors contributed equally to this work

*Corresponding authors, E-mail: zt@xmu.edu.cn; xupeng77@xmu.edu.cn

(Shang et al., 2007), and *cbfa-1* (Marks and Odgren, 2002), have been mapped and linked to body shape divergence across diverse taxa. In addition to structural regulators, endocrine pathways contribute indirectly to morphological outcomes. Hormones associated with the insulin-like growth factor (IGF) axis, such as glucocorticoids (Azetsu et al., 2019), and thyroid hormones (Shkil et al., 2012), have been shown to indirectly modulate growth dynamics and skeletal patterning in fish. The complexity and diversity of these genetic factors pose significant challenges in fully deciphering the molecular basis of body shape differentiation. Consequently, the establishment of populations with well-defined and stable body shape variation remains essential for robust identification of causal genes or single-nucleotide polymorphisms (SNPs), thereby enabling a more precise understanding of the genetic mechanisms underlying body shape evolution in fish.

Carp ranks among the earliest domesticated fish, with breeding practices extending back over 8 000 years (Nakajima et al., 2019). Long-term artificial selection, both intentional and unintentional, has driven extensive morphological diversification within this lineage, leading to the emergence of diverse domesticated forms distinguished by body conformation, scale patterns, and coloration. These include Yellow River carp (YR, *Cyprinus carpio haematopterus*), Hebao red carp (HB, *Cyprinus carpio wuyuanensis*), mirror carp (*C. carpio var. specularis*) (Geri et al., 1995), and naked carp (*Gymnocypris przewalskii*) (Tong et al., 2015). China, as the origin of carp domestication, harbors rich genetic resources encompassing numerous phenotypically distinct lineages. Among these varieties, YR and HB exhibit especially pronounced differences in body shape and are widely used in hybrid breeding programs (Chen et al., 2024). YR retains ancestral traits such as a gray pigmentation and elongated body shape, whereas HB displays vivid red coloration and a compact, “purse-like” morphology defined by reduced head and tail dimensions and increased body depth. Our previous work identified mutations in *mitf* as the primary driver of their body color differences (Li et al., 2023). Building on this foundation, the present study aimed to resolve the genetic determinants underlying their divergent body shape.

Although early hypotheses proposed that the distinctive morphology of HB may stem from impaired calcification of axial structures, resulting in vertebral compression and deformation (Deng, 1981), the genetic determinants remain unclear. To investigate the genetic basis of this phenotype, a hybrid family was established by crossing HB with YR, followed by genome-wide association studies (GWAS) in both the hybrid (F1) and backcrossed (F2) generations. To complement genotypic mapping, transcriptomic profiling was conducted to identify expression signatures associated with body shape variation. Functional validation was performed through targeted gene knockout to assess the developmental impact of candidate loci. In summary, this research elucidates the morphological and molecular framework underlying the unique body architecture of HB and provides mechanistic insight into the genetic regulation of skeletal development and body shape diversification in fish.

MATERIALS AND METHODS

Ethics statement

All animal experiments were carried out in accordance with the Laboratory Animal Care and Use Guidelines and were approved by the Laboratory Animal Experiment Committee of the School of Ocean and Earth Sciences, Xiamen University (Approval No. 2025003).

Hybrid family construction and sample collection

All experimental procedures were conducted at the Carp Breeding Base of the Henan Institute of Aquatic Science. In April 2018, six hybrid families were generated through reciprocal crosses between HB and YR, comprising three direct crosses and three reverse crosses (one male and one female per pair). Two families with high offspring survival—one direct cross (YR♂×HB♀, designated F5) and one reverse cross (YR♀×HB♂, designated F18)—were selected for further propagation. In April 2021, sexually mature individuals from the F1 generation were used to produce F2 offspring through self-fertilization and backcrossing with parental stocks. The F2 cohort included eight self-cross families, two YR backcross families, and 13 HB backcross families. Of these, 10 families survived until 18 months of age and were retained for downstream analyses (Supplementary Table S1). At six months of age, each fish was individually tagged using a passive integrated transponder (PIT) tag for identity tracking, resulting in 212 and 1 290 tagged individuals from the F1 and F2 generations, respectively. Morphometric data were collected at both 6 and 18 months of age using standardized protocols (Jiang et al., 2021; Ming et al., 2009). Total length was measured from the tip of the snout to the end of the caudal fin; body length was measured from the tip of the snout to the base of the caudal fin; head length was measured from the tip of the snout to the posterior edge of the operculum; and body depth was measured as the vertical distance from the anterior base of the dorsal fin to the base of the abdomen.

Artificial insemination and fry rearing were performed under controlled conditions. Sexually mature fish broodstock were maintained in cement holding tanks at 24°C. Females were intraperitoneally injected with LHRH-A2 (4 μg/kg) and HCG (800 IU/kg), while males received half the dose. A second injection was administered 12 h later. Upon ovulation or milt release, the urogenital opening was dried, and gametes were collected by gentle abdominal pressure. Fertilization was conducted by mixing gametes in clean water and spreading the mixture on palm leaves for 30 min. Unfertilized eggs were washed off, and fertilized eggs were transferred to 24°C incubation tanks. Incubation was conducted under stable water temperature and oxygen conditions, with methylene blue added to prevent fungal growth. Upon hatching, larvae were initially fed egg yolk and subsequently transferred to outdoor net cages for further rearing.

Morphometric trait analysis

The body length-to-body depth ratio represents a widely adopted metric for quantifying body shape variation in carp, enabling discrimination between short, rounded types and more elongated individuals (Chiang et al., 1963). Based on this index, morphometric traits were statistically compared across age groups and generations. All measurements and trait correlations were analyzed using R (v.4.3.1). Descriptive statistics, including mean, standard deviation, maximum, and minimum, were calculated for each trait. Visualization of trait distributions, scatter relationships, and trend fitting was performed using the ggplot2 (v.3.4.2) package. Pearson correlation coefficients between traits were calculated using the cor.test function, and composite figure generation and

annotation were conducted using the cowplot (v.1.1.2) package. Differences in morphometric traits among families were evaluated using the LSD.test function with Bonferroni-adjusted *P*-values (*p*.adjusted="bonferroni", alpha=0.05).

DNA extraction, sequencing, and genotyping

Whole-genome resequencing was conducted on 18 HB and 16 YR individuals randomly sampled from natural populations, along with 117 F1 and 427 F2 individuals from hybrid populations. DNA extraction and paired-end library construction were performed by BGI-Qingdao, and sequencing was carried out using the MGISEQ-2000RS platform (China). Each individual yielded approximately 6 Gb of sequencing data, with average raw read coverage of 10× for natural populations and 5× for hybrid populations. Paired-end reads were quality-trimmed and aligned to the HB reference genome using the Burrows-Wheeler Aligner (BWA v.7.17) with default parameters. BAM files were generated using SAMtools (v.1.21) and sorted with Picard (v.3.3) tools (Li & Durbin, 2010). Duplicate reads mapping to identical genome positions were marked and removed using MarkDuplicates in Picard to avoid interference with variant detection. After alignment, variant calling was performed using the HaplotypeCaller module in GATK (v.4.0), and low-quality SNPs and insertions/deletions (indels) were filtered according to GATK best practices (Poplin et al., 2018). Further filtering was performed using VCFtools (v.4.0) to retain variants meeting the following criteria: (1) minor allele count and maximum missing count <2 and (2) biallelic variants only. Final variant annotation was performed using ANNOVAR (Wang et al., 2010).

GWAS and recombination mapping on chromosome A08

Population structure was evaluated via principal component analysis (PCA) using PLINK (v.2.0). GWAS targeting the body length-to-body depth ratio in F1 and F2 populations was performed using the mixed linear model (MLM) implemented in GEMMA (v.0.981) (Zhou & Stephens, 2012). The model incorporated family pedigree, a kinship matrix, and the first three principal components (PCs) as covariates. Wald tests were used to assess statistical significance, and *P*-values were adjusted using Bonferroni correction. Manhattan and quantile-quantile (QQ) plots were generated with the CMplot (v.1.0) package in R (Yin et al., 2021). To identify regions of genomic differentiation and recombination, genome-wide SNP data were analyzed using a sliding window approach (window size: 40 kb; step size: 10 kb). Genomic regions exhibiting strong divergence in allele frequency (F_{ST}) and nucleotide diversity (π ratio) between HB and YR were identified. Candidate regions were defined as those within the top 0.5% of both F_{ST} (>0.315) and log(π ratio) (>0.486) distributions.

Focused analysis on chromosome A08 was carried out to detect potential recombination events and resolve haplotype structure. SNPs showing fixed allele frequency differences (ΔAF>0.95) between HB and YR were selected as parental haplotype markers. Based on these markers, individuals were assigned to one of three haplotype categories: S1S1 (HB haplotype), S2S2 (YR haplotype), or S1S2 (heterozygote). Genotypes from 427 F2 individuals were classified accordingly, and recombination patterns from parents to offspring were reconstructed. Phenotypic comparisons of the body length-to-body depth ratio across haplotype groups were performed using appropriate statistical tests.

Transcriptome profiling of vertebral tissue and differential expression analysis

To investigate haplotype-dependent gene expression within the candidate region, transcriptome sequencing was performed on vertebral tissue samples collected from 1.5-year-old carp individuals representing each of the three haplotype groups (*n*=5 per group; total *n*=15). RNA extraction, library construction, and sequencing were conducted by BGI Genomics (China). High-quality RNA was used to generate DNBSEQ mRNA libraries, followed by paired-end (150 bp) sequencing on the DNBSEQ platform. Raw reads were filtered with SOAPnuke (v.2.17) using the parameters -n 0.01 -l 20 -q 0.4 --adaMR 0.25 --ada_trim --polyX 50 to remove adapters and low-quality bases. Clean reads were processed through a standardized RNA sequencing (RNA-seq) pipeline consisting of Hisat2 (v.2.1.0), StringTie (v.2.1.3), and Ballgown (v.2.3). Specifically, reads were aligned to the HB reference genome using Hisat2 with the -dta option to retain splicing information, then converted to BAM format and sorted using SAMtools. Transcript assembly and quantification were performed using StringTie. Coding sequences (CDS) were predicted and annotated using TransDecoder (v.5.70) (https://github.com/TransDecoder/TransDecoder) to identify functional genes potentially modulated by haplotype variation. PCA and sample correlation heatmaps were generated using DESeq2 (v.2) in R. Expression levels of six candidate genes were extracted, and statistical comparisons among haplotype groups were conducted. Bar plots were generated to visualize differential expression patterns.

Guide RNA (gRNA) design and synthesis

Given the prolonged sexual maturation cycle of carp, functional validation of the *rfln* gene, implicated in body shape development, was conducted in zebrafish (*Danio rerio*), a well-established cyprinid model. Zebrafish harbor two paralogous copies, *rflna* and *rflnb*, which were independently targeted following the protocol described by Yan et al. (2022). Target sequences were designed using CHOPCHOP (Labun et al., 2019), with gRNAs directed to exon 2 of *rflna* and exon 1 of *rflnb*. Forward primers incorporating the T7 promoter and gene-specific targeting sequences (excluding the PAM (NGG) site) were synthesized and combined with a universal reverse primer to generate gene-specific oligonucleotide sequences. *In vitro* transcription was performed under RNase-free conditions using the HiScribe T7 Quick High Yield RNA Synthesis Kit (NEB #E2040, USA), and the synthesized RNA was purified using a Monarch RNA Cleanup Kit (NEB #T2040L, USA). The concentration and purity of the single gRNAs (sgRNAs) were measured using a Nanodrop spectrophotometer (Thermo Scientific, USA) and agarose gel electrophoresis (Bio-Rad). Validation primers targeting the editing regions were designed using the NCBI Primer-BLAST tool (https://www.ncbi.nlm.nih.gov/tools/primer-blast/). All sequences were synthesized by Sangon Biotech (China), and are shown in Supplementary Table S2.

Generation of *rflna*$^{-/-}$*rflnb*$^{-/-}$ zebrafish and phenotypic characterization

Cas9 protein (250–300 pg/nL) and synthesized gRNA (25–35 pg/nL) were mixed in equal volumes and microinjected (1–2 nL per embryo) into one-cell stage embryos of the wild-type AB strain. Control embryos were injected with an equal volume of DEPC-treated water. Genomic DNA was extracted from surviving F0 embryos and controls for polymerase chain

reaction (PCR) amplification. Genome editing efficiency was evaluated using the T7 endonuclease I (T7EI) assay, following the method of Zhong et al. (2016).

Separate CRISPR/Cas9 knockouts of *rflna* and *rflnb* were constructed based on the method of Liu et al. (2018). Microinjections were performed in distinct batches to induce frameshift mutations in each gene. The resulting F0 mosaic individuals were raised to sexual maturity and crossed with wild-type zebrafish to generate F1 offspring. Individuals carrying the same frameshift mutations were screened, and F1 males and females with the same mutation were crossed to obtain F2 homozygous mutants (*rflna*$^{-/-}$ or *rflnb*$^{-/-}$). To obtain double homozygous mutants (*rflna*$^{-/-}$*rflnb*$^{-/-}$), homozygous individuals from the *rflna*$^{-/-}$ and *rflnb*$^{-/-}$ lines were first crossed to produce F1 double heterozygotes (*rflna*$^{+/-}$*rflnb*$^{+/-}$), which were subsequently intercrossed. Genotypes were confirmed by PCR amplification of the target sites, and Sanger sequencing was performed by Sangon Biotech (China). Phenotypic assessments were conducted under a Nikon ECLIPSE Ni-U microscope (Japan), and whole-body images were acquired using a Canon EOS 7D digital camera with a Canon EF 100 mm macro lens (Japan).

Computed tomography (CT) imaging of carp and zebrafish skeletons

Normal 21-month-old YR and HB individuals were randomly selected for skeletal imaging. After anesthesia with MS-222, fish were positioned laterally (left side facing upward) and scanned using a Neusoft CT scanner (China). Scanning was conducted under standardized settings of 120 V X-ray voltage and 254 μA current. Three-dimensional (3D) reconstruction and segmentation of skeletal structures were performed using 3D Slicer (v.5.2.1). DICOM files and CT attenuation values were used to reconstruct whole-body skeletal elements and cross-sectional anatomy. Bone density was inferred from CT values, which exhibit a linear positive correlation with mineralization, and was visualized using density-dependent color mapping.

For zebrafish imaging, three-month-old wild-type and *rflna*$^{-/-}$*rflnb*$^{-/-}$ individuals were anesthetized with MS-222 and scanned using the SkyScan 1272 micro-CT system (Belgium) with the left side oriented upward. Scanning parameters were set to 60 kV voltage and 166 μA current. After 3D reconstruction and visualization, osteophyte bone volume was analyzed using SkyScan 1272.

RESULTS

Variations in morphometric traits of hybrid carp across age groups and generations

To examine temporal dynamics of body shape and evaluate trait correlations across developmental stages, morphometric data were collected from both F1 and F2 generations of hybrid carp (Supplementary Table S3). In a representative dataset of 563 F2 individuals, body weight, body length, body depth, and body length-to-body depth ratio were quantified at 6 and 18 months of age (Figure 1A–D). All four traits exhibited significant correlations between the two time points, with moderate correlation coefficients: body weight (R=0.50, P<2.2e-16), body length (R=0.661, P<2.2e-16), body depth (R=0.50, P<2.2e-16), and body length/body depth ratio (R=0.55, P<2.2e-16).

The body length-to-body depth ratio serves as a key index to distinguish elongated from deep-bodied phenotypes and constitutes a critical selection parameter in the breeding of HB. At 6 months of age, this ratio showed minimal variation across the population, indicating limited morphological differentiation. However, by 18 months of age, significant divergence in body shape had emerged, suggesting that early-stage measurements may not reliably predict adult morphology. The ratio at 18 months of age ranged from 2.87 to 3.99 in YR and from 2.02 to 2.93 in HB, highlighting pronounced interstrain differences. In hybrid offspring, clear segregation of body shape traits was evident. The F1 generation exhibited ratios ranging from 1.72 to 3.63, while the F2 generation ranged from 1.87 to 3.57 (Figure 1E), encompassing both elongated and compact morphotypes (Supplementary Table S4 and Figures S1, S2).

GWAS analysis of body shape traits

To investigate the genetic basis underlying body shape segregation in carp, whole-genome resequencing was performed on 117 F1 individuals and 427 F2 individuals. A total of 2 920 310 SNPs were identified in the F1 population and 2 837 749 SNPs in the F2 population. PCA verified genotypic accuracy, with clustering patterns consistent with known pedigree information. In the F1 dataset, PC1 and PC2 explained 13.9467% and 1.5627% of the total variance, respectively, while in the F2 dataset, PC1 and PC2 explained 19.2811% and 16.9426% of the variance, respectively (Supplementary Figure S3A, B).

GWAS analysis was conducted on both F1 and F2 cohorts, which displayed clear segregation of body shape phenotypes. A QTL region on chromosome A08 exhibited a strong association with variation in the body length-to-body depth ratio. In the F1 population, 489 SNPs were significantly associated with this trait (P<1.77e-7), with 488 SNPs located on chromosome A08, spanning A08: 2 959 631–21 969 637 and encompassing 1 043 genes (Figure 2A). In the F2 population, 5 018 significant SNPs were detected (P<1.76e-8), including 4 266 SNPs located on chromosome A08, spanning A08: 6 846 100–26 388 943 and encompassing 1 025 genes (Figure 2B).

Genomic divergence between HB and YR carp

Signatures of adaptive evolution and artificial selection often manifest as localized divergence within the genome. Moderate genetic differentiation was observed between HB and YR populations, with a genome-wide F_{ST} value of 0.14. Population genetic analyses identified 231 windows exhibiting significant selection signals across chromosomes A06, A08, A16, B05, and B06, encompassing a total of 138 genes (Supplementary Table S5). Notably, a 1.27 Mb interval on chromosome A08 (15.99–17.26 Mb) showed strong genetic differentiation signals (F_{ST}=0.38), coupled with markedly reduced nucleotide diversity in HB (π=0.001076) compared to YR (π=0.005258) (Figure 3A). Within this divergent region, 94 SNPs exhibited near-complete fixation (ΔAF>0.95). Based on the recombination patterns within this region, 18 distinct haplotype combinations were identified and used to classify 427 F2 individuals. These haplotypes were further grouped into three genotype categories: S1S1 (comprising HB-derived haplotypes across all sub-regions), S2S2 (comprising YR-derived haplotypes), and S1S2 (heterozygotes with a mixture of parental haplotypes).

Integration of GWAS results from both F1 and F2 generations identified a 15.99–16.39 Mb segment on

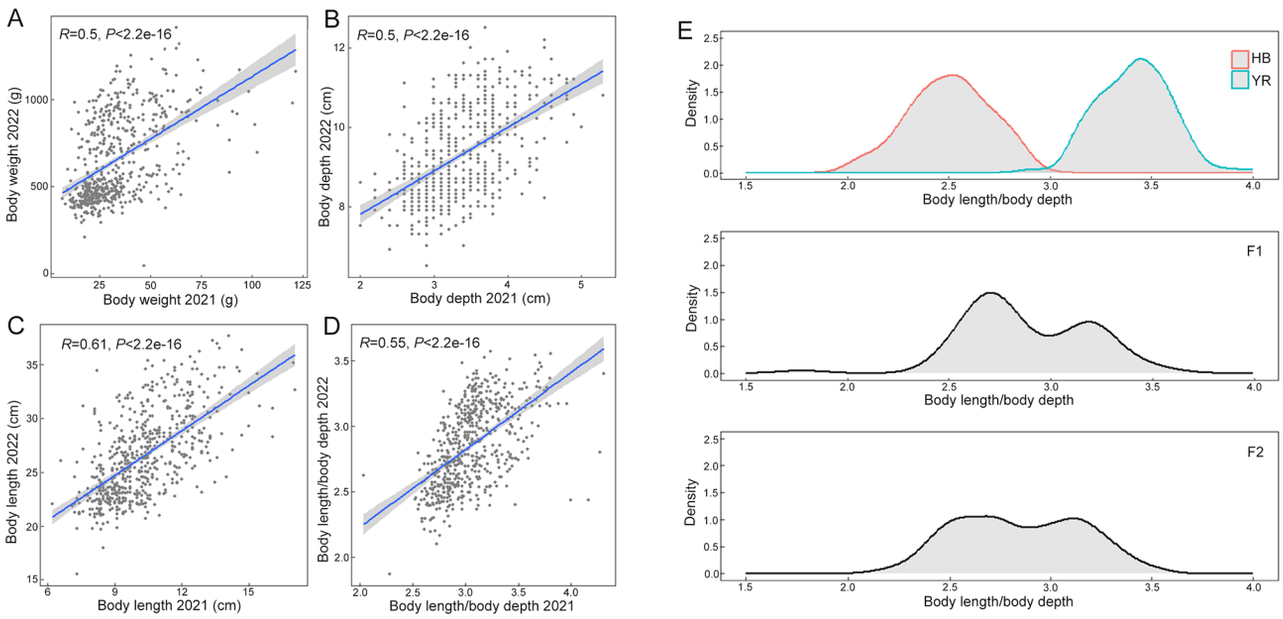

Figure 1 Correlations of body shape traits across age groups and population-level distribution of the body length-to-body depth ratio

A: Correlation of body weight between 6-month-old and 18-month-old individuals; B: Correlation of body depth between 6-month-old and 18-month-old individuals; C: Correlation of body length between 6-month-old and 18-month-old individuals; D: Correlation of body length-to-body depth ratio between 6-month-old and 18-month-old individuals; E: Correlation analysis of body length-to-body depth ratio in 18-month-old individuals, showing distribution and differences between Hebao red carp and Yellow River carp populations, along with distributions in F1 and F2 hybrid offspring.

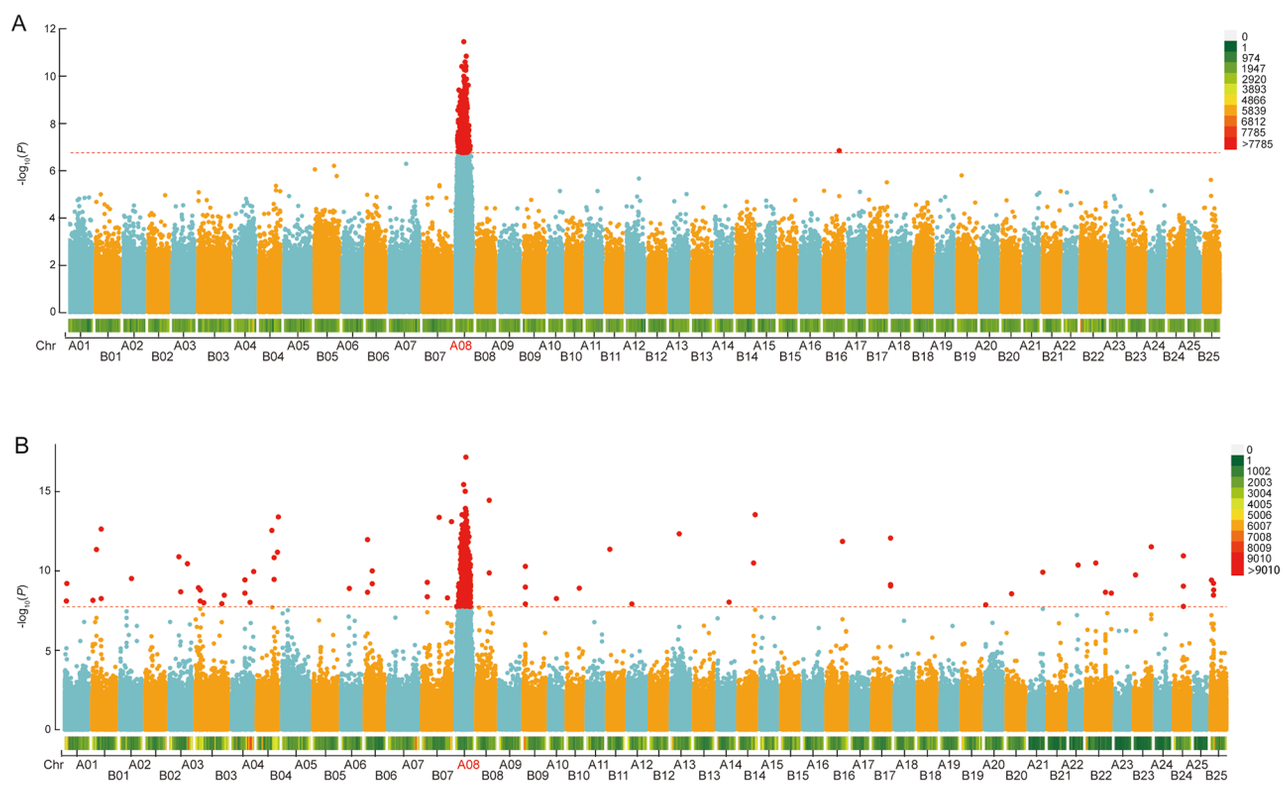

Figure 2 Genome-wide association analysis of body shape variation across populations

A: Genome-wide association analysis of individuals exhibiting body shape variation in the F1 population; B: Genome-wide association analysis of individuals exhibiting body shape variation in the F2 population.

chromosome A08 that was consistently associated with body shape traits in carp. This region contained 45 significant SNPs and exhibited a clear gradient effect among different haplotype genotypes (S1S1, S1S2, and S2S2), with corresponding body length-to-body depth ratios following the pattern S2S2>S1S2>S1S1 (Figure 3B, C). Six genes located within this region (*rimb2*, *agrd1*, *ulk1a*, *ep400*, *ncor2*, and *rflna*) were identified as candidate regulators of body shape variation.

Candidate gene localization for body shape regulation

To identify regulatory genes underlying body shape variation, transcriptome sequencing was performed on vertebral tissue

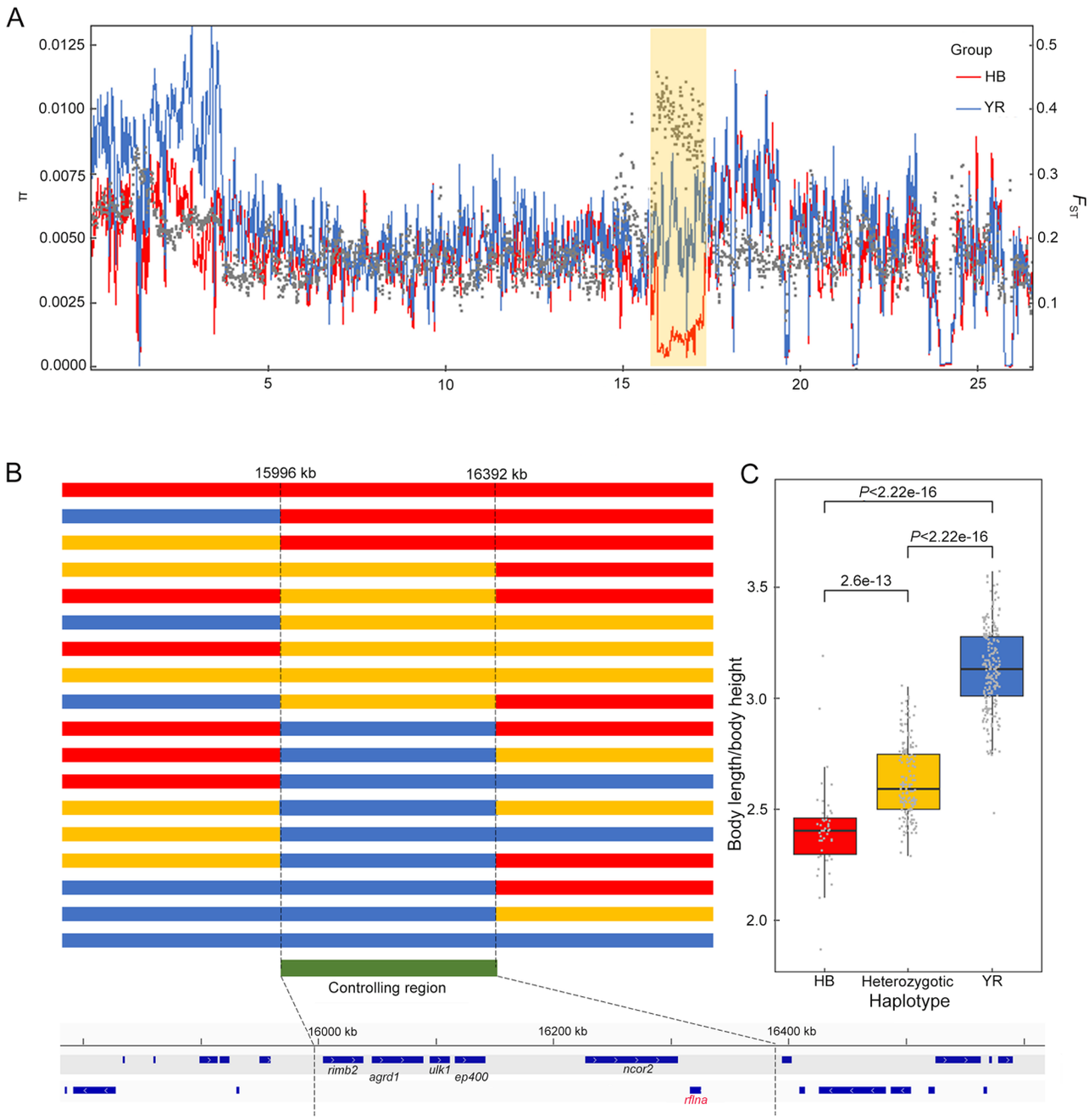

Figure 3 Selective sweep signals and recombination patterns on chromosome A08

A: Nucleotide diversity (π) and population differentiation (F_{ST}) along chromosome A08. X-axis represents genomic positions on chromosome A08. Red and blue lines indicate π values in HB and YR. Highly divergent region spans A08: 15.99–17.26 Mb. B: Genetic architecture underlying abbreviated body shape, Red, blue, and orange bars indicate HB, YR, and heterozygotic genotypes, respectively. C: Body length-to-body height ratio across individuals with different haplotypes.

from 15 F2 individuals representing three genotype classes (S1S1, S2S2, and S1S2), with five biological replicates per group. Each sample generated over 14 Gb of high-quality data. Read mapping to the reference genome achieved an average alignment rate of 90.34%. Differential expression analysis between S1S1 and S2S2 individuals—representing phenotypic extremes—identified 90 differentially expressed genes (DEGs), including 57 down-regulated and 33 up-regulated genes (Figure 4A, B). Kyoto Encyclopedia of Genes and Genomes (KEGG) pathway enrichment analysis indicated significant involvement of genes in developmental signaling pathways, including cell-cell interaction and Wnt signaling (Figure 4C). Expression profiles of six candidate genes (*rimb2*, *agrd1*, *ulk1a*, *ep400*, *ncor2*, and *rflna*) within the QTL region on chromosome A08 were further examined. While no significant differences were detected among genotype groups, both *ulk1a* and *rflna* exhibited a genotype-dependent expression gradient (S1S1>S1S2>S2S2) (Supplementary Figure S4). Notably, 10 body shape-associated SNPs were identified within the CDS region of *rflna*, implicating it as a potential regulator of morphological differentiation in HB.

Comparative analysis of vertebral morphology in HB and YR and functional validation of *rfln*

Micro-CT scanning and morphological assessment

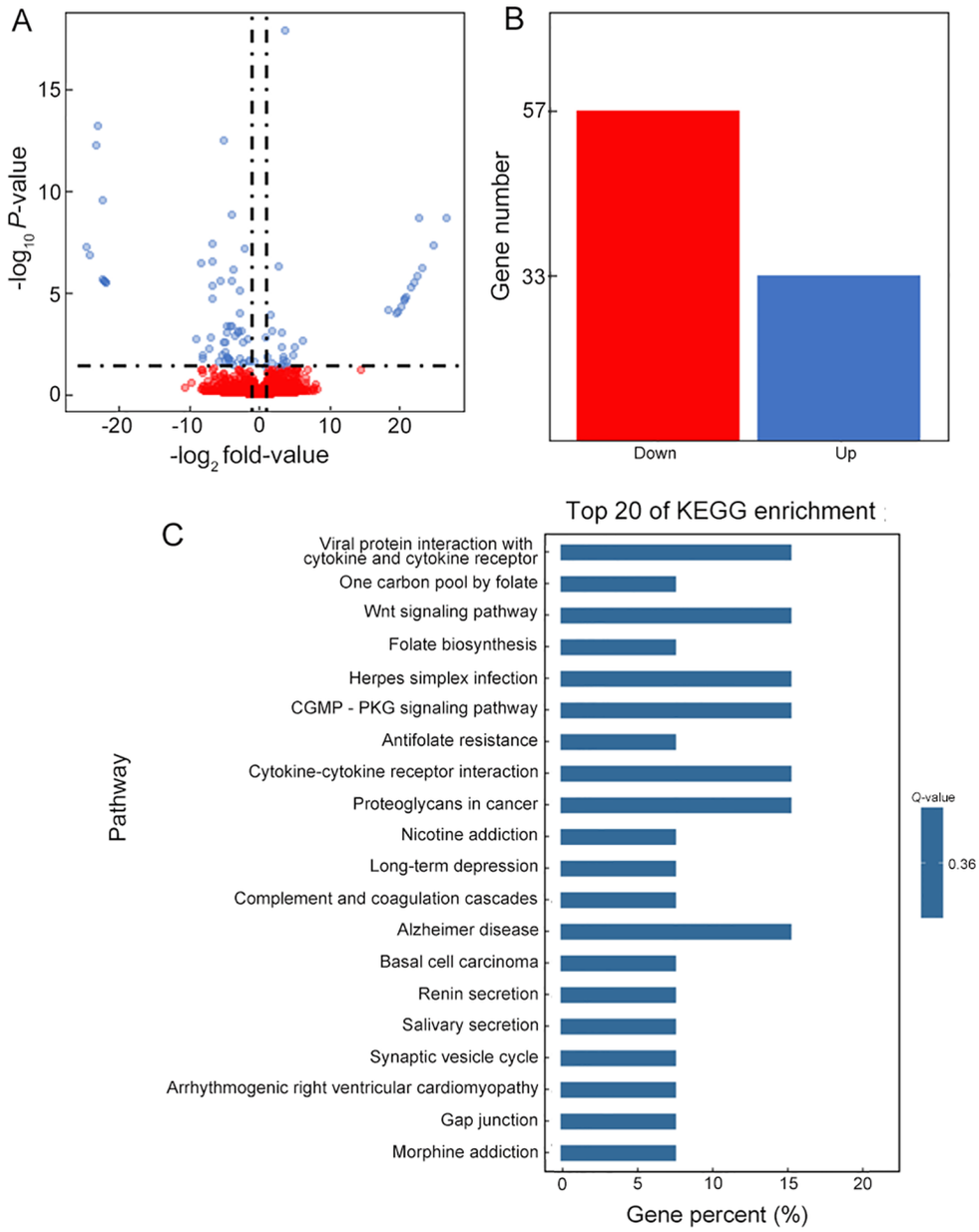

Figure 4 Differentially expressed genes (DEGs) between S1S1 and S2S2 samples

A: Volcano plot showing distribution of genes based on statistical significance (*P*-value) and fold change. B: Number of DEGs. C: Enriched signaling pathways associated with DEGs.

(Figure 5A) revealed that although 18-month-old YR and HB individuals share the same number of vertebrae (35), marked structural differences were detected between the two strains. In HB, vertebrae showed pronounced compression, reduced centrum length, and varying degrees of intervertebral fusion (Figure 5B, C).

To investigate the genetic basis of these phenotypic differences, functional validation of the candidate gene *rfln* was conducted in zebrafish. Given the presence of two paralogous copies, *rflna* and *rflnb*, and the potential for compensatory effects, CRISPR-Cas9 was used to generate double-knockout mutants. Homozygous *rflna*$^{-/-}$*rflnb*$^{-/-}$ zebrafish were successfully obtained (Figure 5D), with editing efficiencies of 50.56% and 31.95% for *rflna* and *rflnb*, respectively (Supplementary Figure S5). Sequencing confirmed a 2 bp deletion in exon 2 of *rflna* and a 3 bp deletion in exon 1 of *rflnb* (Supplementary Figure S6). Notably, neither *rflna*$^{-/-}$ nor *rflnb*$^{-/-}$ single-gene homozygous mutants exhibited any observable skeletal abnormalities compared to control zebrafish. In contrast, *rflna*$^{-/-}$*rflnb*$^{-/-}$ individuals lacked a pair of ribs, exhibited lateral rib flaring, and developed a rounded abdominal profile similar to that of HB. These fish also showed vertebral malformations, including dorsal curvature and significant shortening of vertebrae in the posterior trunk, from the anal to caudal fin region (Figure 5E, F). The mean body length-to-body depth ratio was 3.49±0.21 in controls and 2.94±0.25 in the *rflna*$^{-/-}$*rflnb*$^{-/-}$ mutants. This phenotype closely parallels that of HB, providing strong evidence that *rfln* plays a central role in shaping axial skeletal morphology and contributes to body shape differentiation in carp.

DISCUSSION

As the center of origin for common carp domestication, China maintains extensive genetic diversity across carp lineages,

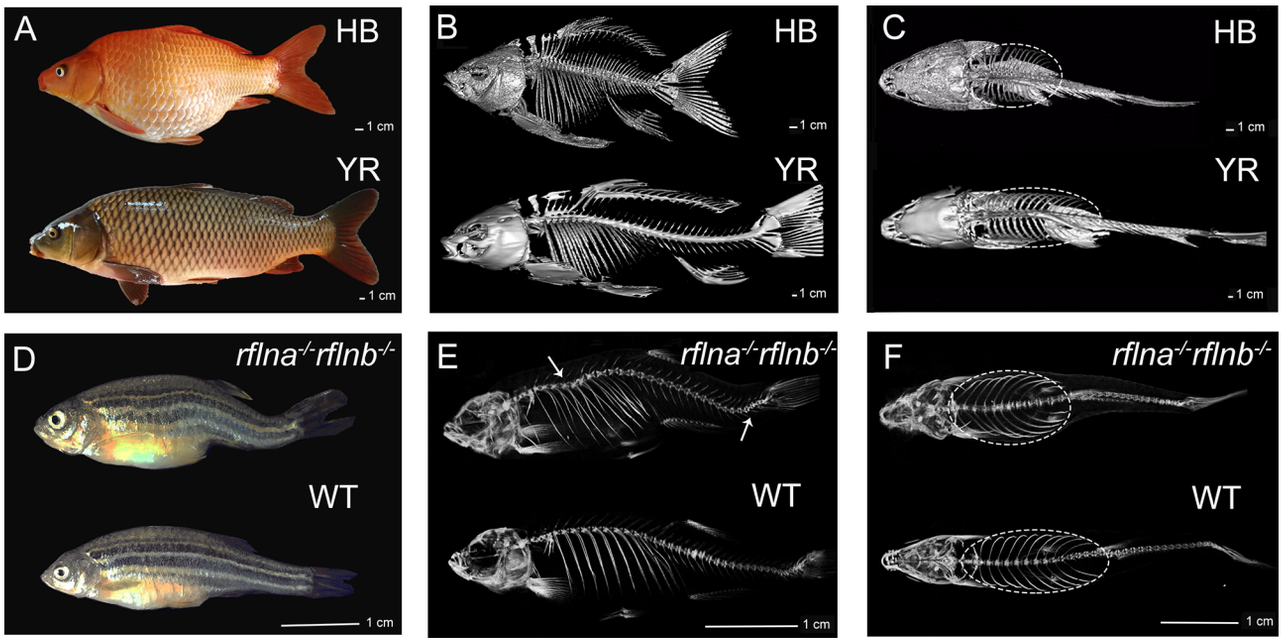

Figure 5 Morphological divergence between carp varieties and phenotypic characterization of body shape and skeletal architecture in *rflna*$^{-/-}$*rflnb*$^{-/-}$ zebrafish

A: Body shape comparison between HB and YR. B: Lateral skeletal structure differences between HB and YR. C: Dorsal skeletal view highlighting differences between HB and YR (dashed line delineates abdominal shape formed by ribs). D: Morphological comparison between *rflna*$^{-/-}$*rflnb*$^{-/-}$ and wild-type zebrafish. E: Lateral skeletal differences between *rflna*$^{-/-}$*rflnb*$^{-/-}$ and wild-type zebrafish (arrow indicates vertebral fusion area). F: Dorsal skeletal view comparing *rflna*$^{-/-}$*rflnb*$^{-/-}$ and wild-type zebrafish (dashed line delineates abdominal shape formed by ribs).

with HB and YR representing two morphologically divergent forms (Li et al., 2023). Body shape plays a central role in fish domestication and serves as a critical parameter for selecting individuals with enhanced performance traits. In this study, GWAS analysis of segregating hybrid progeny derived from HB and YR revealed a major QTL on chromosome A08 linked to variation in body length-to-body depth ratio. By integrating population-level genomic differentiation with transcriptomic profiling across defined genotype groups (S1S1, S1S2, and S2S2), *rflna* emerged as a candidate gene exhibiting marked expression differences among individuals with different body types. Functional validation of *rfln* via CRISPR-Cas9-mediated double knockout in zebrafish demonstrated that disruption of both paralogs led to axial skeletal alterations and body morphology closely resembling HB. These findings establish *rfln* as a key regulator of body shape and contribute to a broader understanding of the genetic and developmental architecture underlying morphological evolution in cyprinid fish.

Body shape variation in vertebrates is often driven by axial skeletal modifications, including increased thoracolumbar vertebral count or the fusion of adjacent vertebrae—processes that exhibit distinct evolutionary patterns across taxa (Masharawi et al., 2008; Witten et al., 2006). In fish, morphological remodeling frequently involves alterations in vertebral column architecture, with at least 26 species across 15 families exhibiting body shape variation linked to axial skeletal changes (Golubtsov et al., 2021). Among anguilliform species, elongation or compression of the body is largely attributable to variation in vertebral number and centrum length. In *Carapus homei*, a reduction in vertebral length and size is associated with increased bone decalcification and soft tissue degeneration, ultimately producing a compact body profile (Parmentier et al., 2004). In Atlantic salmon, long-term domestication-induced body shortening is linked to deformation of poorly mineralized vertebral trabeculae, which disrupt chondrogenesis within the marrow cavity (Witten et al., 2009). In the present study, HB and YR possessed the same number of vertebrae (35) but exhibited strikingly divergent body shapes, suggesting that body shape differences arise independently of vertebral number. HB individuals displayed pronounced axial skeletal abnormalities, characterized by centrum shortening and partial fusion of vertebrae. These features are consistent with earlier observations (Deng, 1981) suggesting that body shape differences between HB and other carp lineages result from impaired vertebral calcification and associated structural degeneration rather than numerical changes in vertebral segmentation. These findings provide strong evidence in support of the conclusions drawn in our study regarding body shape variation between HB and YR.

Deciphering the genetic underpinnings of phenotypic diversity remains a central objective in evolutionary research (Sahni et al., 2013). A major challenge lies in uncovering the sources of genomic variation that give rise to novel and complex traits. In this context, hybridization serves as a powerful mechanism for generating rapid and extensive genotypic and phenotypic recombination, providing a dynamic system for dissecting trait architecture (Gutiérrez-Barragán et al., 2025; Payseur & Rieseberg, 2016). While F1 hybrids typically exhibit relatively limited genetic variability due to their uniform genetic backgrounds, F2 populations generated through intercrossing tends to exhibit enhanced recombination and greater trait segregation (Barton, 2001; Debes et al., 2013; Edmands et al., 2005). For example, Li et al. (2025a) demonstrated that F2 oyster progeny displayed increased trait diversity compared to F1 individuals, offering improved resolution for trait selection in aquaculture. In this study, the number of significant SNPs associated with body shape was

over 10-fold higher in the F2 population than in the F1 hybrids, underscoring the higher genetic variation and broader phenotypic distribution of the F2 cohort and its suitability for mapping complex traits.

Advances in high-resolution genomic and transcriptomic analyses have accelerated the identification of causal variants in hybrid fish lineages. In previous work involving HB-derived hybrids, Li et al. (2023) reported that abnormal splicing of *mitfa* contributed to the red skin phenotype. Further population-level analyses of color-segregating backcross hybrids and multi-omics dissection of color traits implicated biallelic *mitfa* mutations on chromosomes A06 and B06, with additive effects driving red coloration in HB. Body shape, a trait of both biological and commercial relevance in aquaculture species, has similarly benefited from genomic approaches. Geng et al. (2017) employed GWAS in backcross progenies of channel catfish (*Ictalurus punctatus*) and blue catfish (*Ictalurus furcatus*), identifying several body shape-associated genes, including *col1a2*, *col17a1*, and *col21a1*, which function in osteogenesis. Likewise, hybridization between blunt snout bream (*Megalobrama amblycephala*) and topmouth culter (*Culter alburnus*) enabled genetic dissection of growth regulation. Luo et al. (2025) linked phenotypic performance of hybrids to interspecific allele recombination, and transcriptomic analysis of 25 F2 individuals led to the identification of 54 genes significantly associated with growth regulation, including *tspan5*. In the present study, marked morphological divergence between HB and YR parental lines resulted in extensive phenotypic variation across F1 hybrids and backcross populations, reflecting extensive segregation of body shape traits. Genome-wide population analysis identified 231 significant selective sweep regions distributed across chromosomes A06, A08, A16, B05, and B06. Notably, the 15.99–16.39 Mb interval on chromosome A08, which contained 45 SNPs, showed a strong association with body shape traits, suggesting that this locus likely harbors key genes involved in axial morphology regulation.

Numerous genes involved in skeletal development have been mapped to QTLs associated with body shape differentiation (Geng et al., 2017), consistent with the fundamental role of the axial skeleton in defining external morphology. The coordinated formation of cartilage and bone is orchestrated by a network of transcription factors, cytokines, growth factors, and extracellular matrix molecules (Abecasis et al., 2000). In this study, six genes located on chromosome A08 displayed a consistent expression gradient across body shape genotypes (S1S1>S1S2>S2S2), with *rflna* exhibiting the most pronounced differential expression, suggesting a key role in regulating body shape formation in HB. As a downstream effector of the TGF-β signaling pathway, *rfln* modulates cytoskeletal remodeling and chondrocyte precursor differentiation, thereby influencing skeletal patterning and morphogenesis. In vertebrates, *rflna* (*cfm2*/*fam101a*) and its paralog *rflnb* (*cfm1*/*fam101b*) encode highly conserved proteins Rfln-a and Rfln-b (Shimizu et al., 2019), which share over 70% amino acid sequence identity and exhibit substantial functional redundancy (Mizuhashi et al., 2014). Recent studies highlight their vital function in organizing the cytoskeleton (Baudier et al., 2018). By interacting with filamin, Rfln shift its activity from promoting loosely branched actin networks to encouraging the formation of tightly bundled filaments. This switch plays a key role in maintaining cytoskeletal structure and dynamic balance. For instance, a recent study by Li et al. (2025b) integrated selective sweep analyses across pony breeds (withers height <1.02 m) and large-bodied horses (>1.65 m), identifying cis-regulatory variation upstream of *rflna* as a driver of premature vertebral fusion and body shape variation. To investigate the functional role of *rflna* in axial morphology, CRISPR-Cas9 was used to generate *rflna*$^{-/-}$*rflnb*$^{-/-}$ zebrafish. Compared to wild-type, double-knockout zebrafish lost a pair of ribs, with the remaining ribs splayed outward, resulting in a rounded abdominal profile. Axial skeletal abnormalities included a prominent dorsal curvature, significantly shortened vertebrae between the pelvic and caudal regions, and increased bone density—phenotypes closely resembling those observed in HB. These findings parallel skeletal malformations previously reported in *rfln* knockout mice (Baudier et al., 2018), supporting a conserved role for *rfln* in vertebral morphogenesis. Collectively, these results not only deepen our understanding of the genetic basis of body shape differentiation in carp but also provide theoretical support for future exploration of the *rfln* gene regulatory network in body shape optimization and molecular breeding strategies in aquaculture.

CONCLUSION

This study explored the genetic basis of body shape differentiation between HB and YR based on an integrative multi-omics framework. High-resolution CT imaging demonstrated that the significant morphological disparity between the two species primarily arose from vertebral shortening and fusion, rather than differences in vertebral count. GWAS analysis of F1 and backcross F2 hybrid populations identified a QTL region on chromosome A08 (15.99–16.39 Mb) significantly associated with body shape traits. Integrating population genetics and transcriptomic profiling pinpointed *rflna* as a key candidate gene within this locus. Functional validation in zebrafish using CRISPR-Cas9 knockout of *rflna* and *rflnb* successfully replicated a rounded, shortened body phenotype similar to that of HB, confirming the pivotal role of *rflna* in axial skeletal regulation. These findings not only uncover the genetic basis of body shape differentiation in carp but also provide new insights into the regulation of skeletal development and morphological diversity in teleost fish.

DATA AVAILABILITY

The whole-genome sequencing and transcriptome data generated in this study have been deposited in the Sequence Read Archive (SRA, BioProject IDs PRJNA1313475, PRJNA1312344, PRJNA1312664, PRJNA1313484, and PRJNA1313496), Science Data Bank (Data DOIs: https://doi.org/10.57760/sciencedb.j00139.00241, https://doi.org/10.57760/sciencedb.27226, and https://doi.org/10.57760/sciencedb.j00139.00249), and Genome Sequence Archive (GSA, CRA028726, CRA030116, CRA028668, CRA028358, and CRA028346). All sequencing datasets are also available from the corresponding author upon reasonable request.

SUPPLEMENTARY DATA

Supplementary data to this article can be found online.

COMPETING INTERESTS

The authors declare that they have no competing interests.

AUTHORS' CONTRIBUTIONS

P.X., T.Z., and N.L. conceived the project and designed the scientific objectives. J.X., Y.H.W., J.X.F., and X.J.L. were responsible for managing

the fish farming base. Z.J., B.J.L., L.C., S.M.H., B.R.W., F.P., and J.X.M. collected and prepared the samples. Z.J. and B.J.L. conducted bioinformatics analysis. Z.J., B.J.L., and L.C. prepared the manuscript. P.X. and T.Z. revised the manuscript. All authors read and approved the final version of the manuscript.

ACKNOWLEDGMENTS

We sincerely thank the Fisheries Engineering Institute, Chinese Academy of Fishery Sciences (Beijing, China), Henan Academy of Fishery Science (Zhengzhou, China), and College of Fisheries, Henan Normal University (Xinxiang, China) for their valuable support in fish farming and sample collection.

REFERENCES

Abecasis GR, Cardon LR, Cookson WOC. 2000. A general test of association for quantitative traits in nuclear families. *The American Journal of Human Genetics*, **66**(1): 279–292.

Azetsu Y, Chatani M, Dodo Y, et al. 2019. Treatment with synthetic glucocorticoid impairs bone metabolism, as revealed by *in vivo* imaging of osteoblasts and osteoclasts in Medaka fish. *Biomedicine & Pharmacotherapy*, **118**: 109101.

Barton NH. 2001. The role of hybridization in evolution. *Molecular Ecology*, **10**(3): 551–568.

Baudier J, Jenkins ZA, Robertson SP. 2018. The filamin-B-refilin axis-spatiotemporal regulators of the actin-*cytoskeleton* in development and disease. *Journal of Cell Science*, **131**(8): jcs213959.

Blanckenhorn WU. 2000. The evolution of body size: what keeps organisms small? *The Quarterly Review of Biology*, **75**(4): 385–407.

Chen L, Li CY, Li BJ, et al. 2024. Evolutionary divergence of subgenomes in common carp provides insights into speciation and allopolyploid success. *Fundamental Research*, **4**(3): 589–602.

Chiang I K, Chu C H, Lin Y T, et al. 1963. A comparison on certain biological characteristics between the common carp and the red "pursecarp". *Acta Hydrobiologica Sinica*, **6**(3): 82–92. (in Chinese)

Clauset A, Erwin DH. 2008. The evolution and distribution of species body size. *Science*, **321**(5887): 399–401.

Debes PV, Fraser DJ, McBride MC, et al. 2013. Multigenerational hybridisation and its consequences for maternal effects in Atlantic salmon. *Heredity*, **111**(3): 238–247.

Deng ZJ. 1981. A study on body shape formation and body color inheritance in Hebao red carp from Wuyuan, Jiangxi Province. *Freshwater Fisheries*, (6): 14, 22. (in Chinese)

Edmands S, Feaman HV, Harrison JS, et al. 2005. Genetic consequences of many generations of hybridization between divergent copepod populations. *Journal of Heredity*, **96**(2): 114–123.

Geng X, Liu SK, Yuan ZH, et al. 2017. A genome-wide association study reveals that genes with functions for bone development are associated with body conformation in catfish. *Marine Biotechnology*, **19**(6): 570–578.

Geri G, Lupi P, Parisi G, et al. 1995. Morphological characteristics and chemical composition of muscle in the mirror carp (*Cyprinus carpio* var. *specularis*) as influenced by body weight. *Aquaculture*, **129**(1-4): 323–327.

Golubtsov AS, Korostelev NB, Levin BA. 2021. Monsters with a shortened vertebral column: a population phenomenon in radiating fish *Labeobarbus* (*Cyprinidae*). *PLoS One*, **16**(1): e0239639.

Gutiérrez-Barragán A, Varela-Romero A, García-De León FJ, et al. 2025. A review of catfish (Siluriformes) hybridization. *Reviews in Fish Biology and Fisheries*, **35**(1): 145–174.

Hoare DJ, Krause J, Peuhkuri N, et al. 2000. Body size and shoaling in fish. *Journal of Fish Biology*, **57**(6): 1351–1366.

Jena N, MartíN-Seisdedos C, Mccue P, et al. 1997. BMP7 null mutation in mice: developmental defects in skeleton, kidney, and eye. *Experimental Cell Research*, **230**(1): 28–37.

Jiang XN, Li CT, Ge YL, et al. 2021. Analysis of correlation between morphological traits and body mass and morphological variation in five varieties of common carp (*Cyprinus carpio*). *Chinese Journal of Fisheries*, **34**(4): 7–14. (in Chinese)

Labun K, Montague TG, Krause M, et al. 2019. CHOPCHOP v3: expanding the CRISPR web toolbox beyond genome editing. *Nucleic Acids Research*, **47**(W1): W171–W174.

Larson G, Piperno DR, Allaby RG, et al. 2014. Current perspectives and the future of domestication studies. *Proceedings of the National Academy of Sciences of the United States of America*, **111**(17): 6139–6146.

Li BJ, Chen L, Yan MZ, et al. 2023. Intercross population study reveals that co-mutation of *mitfa* genes in two subgenomes induces red skin color in common carp (*Cyprinus carpio wuyuanensis*). *Zoological Research*, **44**(2): 276–286.

Li H, Durbin R. 2010. Fast and accurate long-read alignment with Burrows-Wheeler transform. *Bioinformatics*, **26**(5): 589–595.

Li JW, Pan Y, Xing QG, et al. 2025a. Trait segregation and growth characteristics of the F2 generation hybrids between *Crassostrea dianbaiensis* and *C. iredalei*. *Aquaculture International*, **33**(4): 274.

Li XZ, Wang ZH, Zhu M, et al. 2025b. Genomic insights into post‐domestication expansion and selection of body size in ponies. *Advanced Science*, **12**(16): 2413023.

Liu CX, Li CY, Hu CC, et al. 2018. CRISPR/Cas9-induced *shank3b* mutant zebrafish display autism-like behaviors. *Molecular Autism*, **9**(1): 23.

Luo MX, Tai YK, Li MD, et al. 2025. Transcriptome analysis reveals genetic regulation of growth diversity in F_2 intergeneric hybrids of *Megalobrama amblycephala* and *Culter alburnus*. *Aquaculture*, **595**: 741630.

Marks Jr SC, Odgren PR. 2002. Structure and development of the skeleton. *In*: Bilezikian JP, Raisz LG, Rodan GA. Principles of Bone Biology. 2nd ed. San Diego: Academic Press, 3–15.

Masharawi Y, Salame K, Mirovsky Y, et al. 2008. Vertebral body shape variation in the thoracic and lumbar spine: characterization of its asymmetry and wedging. *Clinical Anatomy*, **21**(1): 46–54.

Ming JC, Dong ZJ, Liang ZY, et al. 2009. Analysis of morphological variation in six common carp (*Cyprinus carpio*) populations. *Journal of Guangdong Ocean University*, **29**(6): 1–6. (in Chinese)

Mizuhashi K, Kanamoto T, Moriishi T, et al. 2014. Filamin-interacting proteins, Cfm1 and Cfm2, are essential for the formation of cartilaginous skeletal elements. *Human Molecular Genetics*, **23**(11): 2953–2967.

Nakajima T, Hudson MJ, Uchiyama J, et al. 2019. Common carp aquaculture in Neolithic China dates back 8, 000 years. *Nature Ecology & Evolutionary*, **3**(10): 1415–1418.

Pang H. 1992. Estimation methods for the heritability of threshold traits. *Hereditas*, **14**(6): 37–40. (in Chinese)

Parmentier E, Lecchini D, Vandewalle P. 2004. Remodelling of the vertebral axis during metamorphic shrinkage in the pearlfish. *Journal of Fish Biology*, **64**(1): 159–169.

Payseur BA, Rieseberg LH. 2016. A genomic perspective on hybridization and speciation. *Molecular Ecology*, **25**(11): 2337–2360.

Poplin R, Ruano-Rubio V, DePristo MA, et al. 2018. Scaling accurate genetic variant discovery to tens of thousands of samples. *BioRxiv*, doi: https://doi.org/10.1101/201178.

Pulcini D, Wheeler PA, Cataudella S, et al. 2013. Domestication shapes morphology in rainbow trout *Oncorhynchus mykiss*. *Journal of Fish Biology*, **82**(2): 390–407.

Sahni N, Yi S, Zhong Q, et al. 2013. Edgotype: a fundamental link between genotype and phenotype. *Current Opinion in Genetics & Development*, **23**(6): 649–657.

Shang YC, Wang SH, Xiong F, et al. 2007. Wnt3a signaling promotes proliferation, myogenic differentiation, and migration of rat bone marrow

mesenchymal stem cells. *Acta Pharmacologica Sinica*, **28**(11): 1761–1774.
Shimizu H, Watanabe S, Kinoshita A, et al. 2019. Identification of a homozygous frameshift variant in *RFLNA* in a patient with a typical phenotype of spondylocarpotarsal synostosis syndrome. *Journal of Human Genetics*, **64**(5): 467–471.
Shkil FN, Kapitanova DV, Borisov VB, et al. 2012. Thyroid hormone in skeletal development of cyprinids: effects and morphological consequences. *Journal of Applied Ichthyology*, **28**(3): 398–405.
Tong C, Zhang CF, Zhang RY, et al. 2015. Transcriptome profiling analysis of naked carp (*Gymnocypris przewalskii*) provides insights into the immune-related genes in highland fish. *Fish & Shellfish Immunology*, **46**(2): 366–377.
Wang K, Li M, Hakonarson H. 2010. ANNOVAR: functional annotation of genetic variants from high-throughput sequencing data. *Nucleic Acids Research*, **38**(16): e164.
Wellik DM. 2007. *Hox* patterning of the vertebrate axial skeleton. *Developmental Dynamics*, **236**(9): 2454–2463.
Witten PE, Gil-Martens L, Huysseune A, et al. 2009. Towards a classification and an understanding of developmental relationships of vertebral body malformations in Atlantic salmon (*Salmo salar* L.). *Aquaculture*, **295**(1-2): 6–14.
Witten PE, Obach A, Huysseune A, et al. 2006. Vertebrae fusion in Atlantic salmon (*Salmo salar*): development, aggravation and pathways of containment. *Aquaculture*, **258**(1-4): 164–172.
Wringe BF, Purchase CF, Fleming IA. 2016. In search of a “cultured fish phenotype”: a systematic review, meta-analysis and vote-counting analysis. *Reviews in Fish Biology and Fisheries*, **26**(3): 351–373.
Yan MZ, Li BJ, Wang JY, et al. 2022. Disruption of *mstn* gene by CRISPR/Cas9 in large yellow croaker (*Larimichthys crocea*). *Marine Biotechnology*, **24**(4): 681–689.
Yin LL, Zhang HH, Tang ZS, et al. 2021. rMVP: a memory-efficient, visualization-enhanced, and parallel-accelerated tool for genome-wide association study. *Genomics, Proteomics & Bioinformatics*, **19**(4): 619–628.
Zhong ZM, Niu PF, Wang MY, et al. 2016. Targeted disruption of *sp7* and *myostatin* with CRISPR-Cas9 results in severe bone defects and more muscular cells in common carp. *Scientific Reports*, **6**(1): e22953.
Zhou X, Stephens M. 2012. Genome-wide efficient mixed-model analysis for association studies. *Nature Genetics*, **44**(7): 821–824.